HHS Public Access

Author manuscript

J Proteome Res. Author manuscript; available in PMC 2022 September 28.

Published in final edited form as:

J Proteome Res. 2021 July 02; 20(7): 3475–3488. doi:10.1021/acs.jproteome.1c00093.

Crosstalk of the IκB kinase with spliced X-box binding protein 1 couples inflammation with glucose metabolic reprogramming in epithelial-mesenchymal transition

Yingxin Zhao[1,2,3,*], **Jing Zhang**[1], **Hong Sun**[1], **Allan R Brasier**[4,*]

[1]Department of Internal Medicine, University of Texas Medical Branch (UTMB), Galveston, TX, 77555-1060;

[2]Institute for Translational Sciences, UTMB;

[3]Sealy Center for Molecular Medicine, UTMB

[4]Institute for Clinical and Translational Research, University of Wisconsin-Madison School of Medicine and Public Health, Madison, WI 53705

Abstract

Epithelial-mesenchymal transition (EMT) plays a critical role in airway injury, repair, and structural remodeling. IκB kinase (IKK)-NFκB signaling regulates late EMT-associated genes expression. However, IKK-mediated mesenchymal transition occurs earlier than NFκB/RelA subunit-dependent EMT gene expression, leading us to investigate the hypothesis that IKK plays an independent mechanism in transforming growth factor-beta (TGFβ)-induced EMT. Time-resolved dissection of early proteome and phosphoproteome changes in response TGFβ and a specific IKK inhibitor, BMS-345541, revealed that IKK regulates cascades of 24 signaling pathways essential in EMT, including TGFβ signaling, p38 mitogen associate protein kinase (MAPK), Toll receptor signaling, and integrin pathways. We identified early IKK-dependent phosphorylation of core regulatory proteins in essential EMT signaling cassettes, including ATF2, JUN, NFKB1/p105, and others. Interestingly, we found that IKKβ directly complexes with- and phosphorylates the spliced X-box-binding protein 1 (XBP1s). XBP1s is an arm of the unfolded protein response (UPR) that activates the Hexosamine Biosynthetic Pathway (HBP), a pathway that mediates protein N-glycosylation and survival from ER stress-induced apoptosis in EMT. We found that inhibition of IKK activity abolishes the phosphorylation of XBP1-T48, blocks XBP1s nuclear translocation and inhibits the activation of HBP. Our study elucidates a previously unrecognized IKKβ-XBP1s-HBP crosstalk pathway that couples inflammation and glucose metabolic reprogramming in ETM. Because XBP1-HBP controls N-glycosylation of extracellular matrix (ECM) in EMT, this novel IKKβ-XBP1-HBP pathway may contain therapeutic targets

[*]Corresponding authors: Yingxin Zhao, Ph.D., Tel 409-772-1923, yizhao@utmb.edu; Allan R. Brasier, MD., Tel (608) 263-7371, abrasier@wisc.edu.

Author contributions

YXZ and ARB conceived, designed, and initiated the study. JZ, YXZ, HS, and ARB conducted the experiments. YXZ, JZ, and ARB analyzed the data and interpreted the results. YXZ and ARB wrote the manuscript. All authors read the manuscript and discussed the interpretation of results.

Conflict of interest

The authors declare that they have no conflict of interest.

whose inhibition could prevent ECM remodeling in lung fibrosis or other airway remodeling diseases.

Graphical Abstract

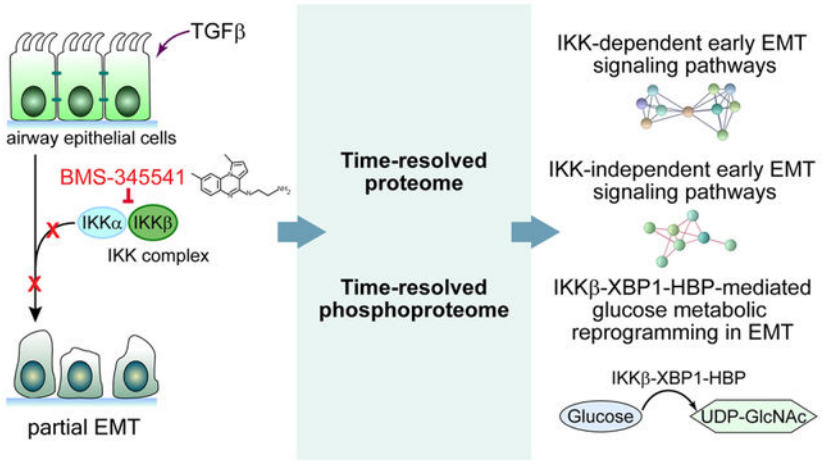

Keywords

epithelial-mesenchymal transition; proteomics; IκB kinase-NFκB; N-glycosylation; extracellular matrix; unfolded protein response; hexosamine biosynthesis pathway

INTRODUCTION

Airway remodeling is a structural alteration of the airways produced by epithelial injury and repair. Epithelial injury induces cellular de-differentiation, affecting mucosal innate inflammatory response and producing fibrogenic cytokines, such as transforming growth factor-beta (TGFβ).[1–4] Ample evidence from various human and mouse models of airway disease indicates that environmental oxidants, aeroallergens, and RNA virus infections can induce epithelial-mesenchymal transition (EMT) in the airway.[5–7] Mesenchymal transition disrupts mucosal barrier function, causes goblet cell metaplasia, enhances the production of extracellular matrix (ECM), and reduces airway compliance and lung function, implying that EMT has significant clinical relevance in airway diseases.[8–9] In particular, enhanced ECM production results in expansion of the *lamina reticularis* is an early pathological feature universally associated with allergic asthma.[7, 10] However, the mechanisms of how epithelial cell state changes induce ECM remodeling are incompletely understood.

Mesenchymal transition involves a series of cell-state changes driven by core mesenchymal regulatory factors, including the Snail family transcriptional repressor (SNAI1) and Zinc Finger E-Box Binding Homeobox (ZEB1).[11–14] Our previous studies revealed that the NFκB pathway is a master regulator of airway inflammation and EMT in primary human small airway epithelial cells (hSAECS).[5, 15–16] We found that NFκB/RelA nuclear translocation occurred after 3 d of TGFβ treatment and directly regulates the gene expression of core transcriptional regulators of EMT, including SNAI1, ZEB1, JUN, and

proteins in the WNT pathway.[16] NFκB/RelA transcription activities are primarily regulated by IκB kinase (IKK) complex, whose catalysis is generally carried out by a heterodimeric kinase consisting of IKKα and IKKβ subunits.[17] Administration of a small-molecule inhibitor of the IKK, BMS-345541, blocks inflammatory response and EMT and prevents airway remodeling.[5, 7] Interestingly, IKK inhibition blocks EMT gene expression programs before substantial NFκB translocation occurs, suggesting that IKK plays an independent, unknown role in regulating the EMT process.

The activation of EMT transcription factors substantially induces the gene expression of ECM proteins. Epithelial cells are not professional secretory cells and produce few ECM proteins under normal conditions. We recently revealed a new molecular mechanism underlying the protein factory's transformation and secretory machinery during the mesenchymal transition.[18] We found that mesenchymal cells activate the X-box binding protein 1 (XBP1)-axis of unfolded protein response (UPR) to allievate the ER stress caused by the increased demand for protein synthesis of ECM. Upon ER stress, inositol-requiring protein 1 (IRE1) triggers unconventional cytoplasmic splicing of XBP1 mRNA and generates an active b-ZIP transcription factor, XBP1s, which translocates into the nucleus to initiate transcriptional programs that upregulate a broad spectrum of UPR-associated genes involved in protein entry into the ER, protein folding, ER-associated degradation (ERAD), and ER biogenesis. Furthermore, our work reveals another critical function of XBP1-URP. We found that mesenchymal transition in hSAECs reprograms glucose metabolism to hexosamine biosynthetic pathway (HBP) via XBP1-mediated UPR.[18] XBP1s is the transcription factor of HBP enzymes, such as glutamine--glucose-6-phosphate transaminase (GFPT)1 and GFPT2. Activation of XBP1-UPR upregulates the gene expression of these enzymes in HBP pathway, shifting the glucose flux from glycolysis to the production of uridine diphosphate N-acetylglucosamine (UDP-GlcNAc), a metabolite donor and mediator of protein N-glycosylation and O-GlcNAcylation. We found that the accumulation of intracellular UDP-GlcNAc increases the protein N-glycosylation of ECM (N-matrisome), which improves ER protein homeostasis and increases ECM secretion.[18] Excessive ECM deposition is a hallmark characteristic of airway remodeling in chronic asthma. It contributes to the stiffness and reduced contractility/relaxation of asthmatic patients' airways[19–22], implying that XBP1-mediated glucose metabolic reprogramming and N-matrisome play essential roles in the pathological changes in the airway remodeling. However, the relationship between the XBP1-HBP-pathway and the IKK-NFκB pathway is unknown.

Here, we carried out time-series proteomics and phosphoproteomics analysis on TGFβ-stimulated hSAECs in the presence or absence of the specific IKK inhibitor, BMS-345541. We found that IKK has a profound regulatory effect on cascades of TGFβ stimulated phosphoproteins early in the mesenchymal transition. We identified the activation of 24 IKK-mediated signaling pathways, including TGFβ signaling, p38 MAPK, Toll receptor signaling, and integrin receptor. We found that XBP1-HBP mediated glucose metabolic reprogramming starts upon partial EMT and is mediated by IKKβ through direct phosphorylation of T48 of XBP1. Our study reveals the vital role of IKK in regulating the EMT process and provides a novel mechanism by which IKK-NFκB promotes ECM

secretion through the XBP1-HBP pathway, revealing a complex crosstalk mechanism between the IKK and XBP1 pathway.

EXPERIMENTAL SECTION

Cell culture

An immortalized primary human small airway epithelial cell line was previously described.[7, 16, 23–26] The immortalized hSAECs were grown in SAGM small airway epithelial cell growth medium (Lonza, Walkersville, MD) in a humidified atmosphere of 5% CO_2. hSAECs were stimulated with TGFβ (10 ng/ml, PeproTech, Rocky Hill, NJ) for 0, 1, and 3 d in the absence or presence of a small molecule IKK inhibitor BMS-345541 (10 μM, Sigma-Aldrich, St. Louis, MO). The dose of BMS 345541 (10 μM) was selected based on previous dose-response titrations in hSAECs. Here, IKK inhibition was determined for 1, 3 and 10 μM of BMS concentrations on IL6 expression[25]; a well-established NFkB-dependent gene. 10 μM was required for full suppression of IL6 expression and was therefore selected because it was the lowest dose that produced complete inhibition of the pathway. This concentration is standardly used and accepted by others in the field[5, 7, 27–29]. Each experimental group had three biological replicates.

Western Immunoblot

The nuclear fractions were extracted using NE-PER™ Nuclear and Cytoplasmic Extraction Reagents (Thermo Scientific). Protein concentration was determined by bicinchoninic acid (BCA, Pierce, Thermo Scientific), and 20 μg were dissolved into SDS loading buffer (with 5% βME) and fractionated on 4−15% Mini-protean TGX gels (BioRad, Hercules CA, USA) in 1× Tris-Glycine SDS (TGS) 1× running buffer at room temperature. Proteins were electro-transferred to nitrocellulose membrane (BioRad, Hercules CA, USA) in 1× TGS buffer-methanol (20%) buffer. The blots were blocked with 3% BSA in TBST (Tris-buffered saline, 0.1% Tween 20) for one hour and incubated overnight at 4 °C in primary antibodies. Antibodies were: XBP-1s (9D11A43) mouse mAb (Biolegend #658802, Danvers, MA), and histone deacetylase 1 (HDAC1) (10E2) moue mAb (Santa Cruz Technology sc-81598, Dallas, TX). Secondary antibodies was IRDye 680RD goat antimouse IgG secondary antibody (Li-Cor 926−68070).

Lectin staining and confocal immunofluorescence microscopy

For confocal fluorescence microscopy, hSAECs were plated over a cover glass (Fisher Scientific, Pittsburgh, PA) in a 6-well plate two days before the experiment. The cells were treated with TGFβ for 0, 1, and 3 d in the presence or absence of BMS-345541, then fixed with 4% paraformaldehyde in PBS for 20 min and incubated with 0.1 M ammonium chloride for 10 min. Then, cells were permeabilized with 0.5% Triton-X100 in PBS, followed by incubation in blocking buffer (5% goat serum, 0.1% IGEPAL CA-630, 0.05% NaN3, and 1% BSA) for one hour, and then incubated with WGA-FITC (20 μg/mL, Sigma, St. Louis, MO) for 1 hour at room temperature. After washing, cells were imaged at the wavelength of 488 nm. Nuclei were stained with DAPI.

Quantification of the cellular UDP-GlcNac

About 1×10^6 cells were homogenized in 0.7 M perchloric acid, and the protein pellets were removed by centrifuging at 15,000 rpm.[30] The resulting supernatants were neutralized with 2 M sodium carbonate. The resulting nucleotide-sugars were desalted using TopTip Carbon (Hypercarb), eluted with 80% ACN and dried under vacuum. Briefly, the desalted nucleotide-sugars were resuspended in 0.01M NH_4OH-40% acetonitrile (ACN) and directly analyzed by LC-SRM-MS. The SRM parameters for UDP-GlcNAc are listed in Supplemental Table S1. LC-SRM-MS analysis was performed with a TSQ Vantage triple quadrupole mass spectrometer equipped with a nanospray source (Thermo Scientific, San Jose, CA), as described previously.[18]

Protein extraction, trypsin digestion, and enrichment of phosphopeptides

The cells were washed three times with PBS solution and collected into a conical tube for centrifugation. The proteins were extracted with Trizol reagent (Invitrogen, Carlsbad, CA) as described previously.[18, 26] The protein pellet was resuspended in 100 μL of 8 M Guanidine HCl. The protein concentration was measured using BCA assay. One milligram of proteins from each sample was processed for digestion. The proteins were first reduced with 10 mM DTT at room temperature for 30 min, followed by alkylation with 30 mM iodoacetamide at room temperature for two hours. The sample was then diluted with 200 μL of 50 mM ammonium bicarbonate (pH 8.0). An aliquot of Lys-C/Trypsin solution (Promega, Madison, WI) was added to each sample at the 50:1 protein: enzyme ratio. The samples were incubated at 37 °C overnight, and the solutions were further diluted with 500 μL of 100 μM of triethylammonium. An aliquot of Trypsin solution (Promega, Madison, WI) was added to each sample at the 50:1 protein: enzyme ratio. The samples were incubated at 37 °C for 16 h. The trypsin digestion was stopped by adding 100 μL of 10% trifluoroacetic acid was added to each sample to stop the trypsin digestion. Ten micrograms of tryptic peptides were desalted on reversed-phase tC18 SepPak columns (Waters, Milford, MA) and analyzed by LC-MS/MS. About 1 milligram of tryptic peptides was used for enriching phosphopeptides. The peptides were dried with speedvac and resuspended in 80% acetonitrile (ACN) and 6% trifluoroacetic acid (TFA) and incubated with TiO_2 beads (GL Sciences Inc. Tokyo, Japan) (1:5 peptides to bead ratio) for 20 min. The beads were washed with 80% ACN, and 0.1% TFA and phosphopeptides were eluted using 5% ammonia.

NanoLC-MS/MS Analysis

The desalted peptides were reconstituted in 20 μl 4% ACN/0.1% formic acid. All peptide samples were separated on an online nanoflow Easy nLC1000 UHPLC system (Thermo Scientific) and analyzed on a Q Exactive Orbitrap mass spectrometer (Thermo Scientific, San Jose, CA). 10 μl of the sample was injected onto a capillary peptide trap column (Acclaim® Pepmap 100, 75 μm × 2 cm, C18, 3 μm, 100 Å, Thermo Scientific). After sample injection, the peptides were separated on a 25-cm UHPLC reversed-phase column (Acclaim® Pepmap 100, 75 μm × 25 cm, C18, 2 μm, 100 Å, Thermo Scientific) at a flow rate of 300 nL/min. A 4-h linear gradient from 2% solvent A (0.1% formic acid in H_2O) to 35% solvent B (0.1% formic acid in ACN) was used for each LC-MS/MS run. The data-dependent acquisition was performed using the Xcalibur 2.3 software in positive

ion mode at a spray voltage of 2.1 kV. Survey spectra were acquired in the Orbitrap with a resolution of 70,000, the maximum injection time of 20 ms, an automatic gain control (AGC) of 1e6, and a mass range from 350 to 1600 *m*/*z*. The top 15 ions in each survey scan were selected for higher-energy collisional dissociation scans with a resolution of 17,500. For all higher-energy collisional dissociation scans, collision energy was set to 28, the maximum inject time was 200 ms, and the AGC was 1e5. Ions selected for MS/MS were dynamically excluded for 30 s after fragmentation.

Identification and quantification of protein and phosphorylation

Mass spectra were analyzed using MaxQuant software (version 1.5.2.8).[31] The initial maximum allowed mass deviation was set to 10 ppm for monoisotopic precursor ions and 0.5 Da for MS/MS peaks. Enzyme specificity was set to trypsin, defined as C-terminal to arginine and lysine excluding proline, and a maximum of two missed cleavages was allowed. Carbamidomethylcysteine was set as a fixed modification and methionine oxidation as variable modifications. For identifying and quantifying protein phosphorylation, phosphorylation on serine, threonine, and tyrosine was set as variable modification. The spectra were searched by the Andromeda search engine against the Human SWISSPORT sequence database (containing 20,193 human protein entries) combined with 248 common contaminants and concatenated with the reversed versions of all sequences. Quantifications were performed with the label-free algorithms in Maxquant.[32] The ‘match between runs’ feature of MaxQuant was used to transfer identifications to other LC-MS/MS runs based on their masses and retention time (maximum deviation 0.7 min), and this was also used in quantification experiments. The detailed parameters for label-free LC-MS/MS quantification and MaxQuant data analysis were listed in Supplemental Table S2. We required at least one ‘razor peptide’ for quantification. The required false positive rate for identification was set to 1% at the peptide level, and 1% at the protein level and the minimum required peptide length was set to 6 amino acids. Contaminants, reverse identification, and proteins only identified by modified peptides were excluded from further data analysis.

Proteomics data analysis and statistical analysis

We used the Perseus platform[33] to analyze the Maxquant output, including statistics, Hierarchical clustering, and principal component analysis (PCA). Reversed identifications and proteins identified only by site modification were strictly excluded from further analysis. For proteomics analysis, proteins identified only by site modification were excluded from further analysis as well. After filtering (3 valid values in at least one group), the remaining missing values were imputed from a normal distribution (width: 0.3 of standard deviation; downshift: 1.8 of standard deviation). Multiple sample ANOVA test with Permutation-based FDR correction and Two-way ANOVA test with Permutation-based FDR was performed to identify the significantly differentially expressed proteins. The unsupervised hierarchical clustering and heat map were based on protein LFQ intensity or the MS intensity of phosphopeptides. The rows of the heat map indicate the proteins, and the columns indicate the samples. The log2 LFQ intensity of each protein was z-score normalized for each row. Hierarchical clustering of the z-normalized log2 LFQ intensity was performed using Euclidean distances between means. The number of clusters was set as 300. Genome ontology enrichment analysis of molecular functions and biological function in differentially

expressed proteins was using Panther (http://pantherdb.org/). This classification uses an evolutionary framework to infer protein functions in a species-independent manner.[34] The resulting *p-values* were adjusted with Bonferroni correction for multiple testing. The significant hits are those with the adjusted p-valve better than 0.05.

Stable Isotope Dilution-Selected Reaction Monitoring-MS

The SID-SRM-MS assays of selected proteins were developed as described previously.[35] For each targeted protein, two or three peptides were initially selected, and then the sensitivity and selectivity of these were experimentally evaluated as described previously. The peptide with the best sensitivity and selectivity was selected as the surrogate for that protein. For each peptide, 3–5 SRM transitions were monitored. The signature peptides and SRM parameters are listed in Supplemental Table S1. The peptides were chemically synthesized, incorporating isotopically labeled [$^{13}C_6{}^{15}N_4$] arginine or [$^{13}C_6{}^{15}N_2$] lysine to a 99% isotopic enrichment (Thermo Scientific, San Jose, CA). The amount of stable isotope-labeled standard (SIS) peptides was determined by amino acid analysis. Each experimental group has at least two biological replicates. The tryptic digests were then reconstituted in 30 μl of 5% formic acid-0.01% TFA. An aliquot of 10 μl of 50 fmol/μL diluted SIS peptides was added to each tryptic digest. These samples were desalted with a ZipTip C18 cartridge and analyzed by liquid chromatography (LC)-SRM-MS a TSQ Vantage triple quadrupole mass spectrometer equipped with a nanospray source (Thermo Scientific, San Jose, CA) as described previously.[18, 26]

All SRM data were manually inspected to ensure peak detection and accurate integration. The chromatographic retention time and the relative product ion intensities of the analyte peptides were compared to those of the stable isotope-labeled standard (SIS) peptides. The variation of the retention time between the analyte peptides and their SIS counterparts should be within 0.05 min, and the difference in the relative product ion intensities of the analyte peptides and SIS peptides were below 20%. The peak areas in the extract ion chromatography of the native and SIS version of each signature peptide were integrated using Xcalibur® 2.1. The default values for noise percentage and base-line subtraction window were used. The ratio between the peak area of the native and SIS version of each peptide was calculated. Student's t-test was performed to determine if the changes in the protein expression were statistically significant.

The mass spectrometry proteomics data have been deposited to the ProteomeXchange Consortium[36] via the PRIDE partner repository with the dataset identifier PXD023531. SRM-MS data have been deposited to PASSEL with the dataset identifier PASS01667.

RESULTS

Time-series Proteomics and phosphoproteomics of hSAECs treated with TGFβ and IKK inhibitor.

Our previous studies found that NFκB is a central transcription factor in TGFβ-induced EMT of primary human small airway epithelial cells.[5, 7, 16, 25] NF-κB/RelA nuclear translocation accumulated significantly only after 3 d of TGFβ stimulation.[5, 16] Chromatin

immunoprecipitation shows that NF-κB/RelA binds and induces the expression of the core EMT regulators (SNAIL, ZEB1, TWIST1), mesenchymal intermediate filaments, (VIM), and ECM components (FN1).[5, 16] Interestingly, IKK inhibition with the selective IKKs inhibitor, BMS-345541[37], potently blocked EMT-associated gene expression before stable NFκB/RelA nuclear translocation was observed. To examine how IKK regulates the early signaling of EMT in hSAECs, we conducted time-series proteomics and phosphoproteomics study on hSAECs treated with TGFβ for 0, 1, and 3 d in the presence or absence of BMS-345541, using doses that block NFκB signaling as described previously[5, 7, 25] (Fig. 1A). This study quantified 3,283 proteins (Supplemental Table S3) and 7,654 phosphopeptides (Supplemental Table S4). Among them, the abundance of 2,508 proteins and 3,926 phosphopeptides showed a group-wised difference (multiple-sample ANOVA test with Permutation-based FDR correction, q-value < 0.01 were statistically significant).

To assess the reproducibility of protein and phosphoprotein quantification among the replicates and obtain an overview of the proteome and phosphoproteome profiles obtained from the six experimental conditions, we performed Principal Component Analysis (PCA) using differentially expressed proteins and phosphopeptides, respectively. As shown in Fig. 1B and 1C, each group's replicates are clustered together, indicating that LC-MS quantification of proteins and phosphopeptides are highly reproducible. Additionally, the PCA scatter plot of protein abundance has six distinct clusters representing six experimental conditions (Fig. 1B), suggesting that TGFβ induces time-dependent protein expression changes. PCA plot also shows that TGFβ/3 d and TGFβ/3 d+BMS groups are far apart, and the same with TGFβ/1 d and TGFβ/1 d+BMS groups, suggesting that inhibition of IKK activity has distinct effects on TGFβ-induced protein expression changes. The PCA analysis of the phosphoproteomics data revealed that the abundance of differentially expressed phosphopeptides could also separate the six experimental groups (Fig. 1C). We found that the hSAECs control group and hSAECs pretreated with BMS-345541 are further separated in the PCA plot of phosphopeptides, while they are close together in the PCA plot of proteins, suggesting that inhibition of IKK has a more substantial impact on the basal level of phosphorylation than that of protein expression.

IKK is a mediator of cascading EMT signaling pathways

We investigated the temporal dynamics of protein phosphorylation in the early stage of TGFβ-induced EMT in the presence or absence of the BMS-345541. The time-series hierarchical cluster analysis of 3,926 significant phosphopeptides resulted in six significant clusters which mostly segregate protein phosphorylation peaking on 0, 1, and 3 days(d) of TGFβ treatment in the presence or absence of IKK inhibitor (Fig 2A), suggesting that TGFβ induced time-dependent protein phosphorylation and many of them were regulated by IKK.

Because protein phosphorylation plays a central role in cell signaling, we focused our analysis of phosphoproteomics data on how IKK mediated EMT signaling pathways. We were especially interested in which TGFβ-activated signaling pathways were regulated by IKK inhibitor. To this end, we conducted the two-way ANOVA analysis on the phosphoproteomics data from hSAECs treated with TGFβ ± BMS-345541 for 1 d and 3 d. With this analysis, we identified 550 phosphopeptides (Supplemental Table S5) that

were significantly regulated by TGFβ and BMS-345541 (two-way ANOVA TGFβ p-value <0.01, two-way ANOVA BMS p-value <0.01, and two-way ANOVA interaction p-value <0.01), including transcription factors, kinases, and other critical proteins important in EMT signaling pathways. For example, we found that TGFβ induced strong early and consistent phosphorylation of S903 and S907 on nuclear factor NF-kappa-B p105 subunit (NFKB1/p105), and IKK inhibitor completely blocked the phosphorylation of these two sites (Fig. 2B). NFKB1/p105 is an essential regulator of Toll receptor signaling and inflammation mediated by chemokine and cytokine stimuli.[17] Phosphorylation of NFKB1-S903/S907 is required for proteolysis of NFKB1 and NFκB transcriptional activity.[38–39] Similarly, we observed that TGFβ-induced phosphorylation on two members of the activator protein 1 (AP-1) transcription factor family, cyclic AMP-dependent transcription factor ATF-2 (ATF2), and transcription factor AP-1 (JUN) (Fig. 2C, D). ATF2 is involved in the TGFβ signaling pathway[40–41], and phosphorylation of T69/T71 is required for its transcription activities.[42] We found that TGFβ induced a 3.4- and 5.5-fold increase in phosphorylation on ATF2-T69/T71 on d 1 and d 3, respectively, and BMS-345541 restored the phosphorylation of these two sites to the basal level. JUN is an important transcription factor of many signaling pathways, such as toll receptor signaling pathway, TGFβ signaling, and inflammation signaling. Phosphorylation of JUN-S63 is required for its transcription activity,[43] and we found that TGFβ induced over a fivefold increase of phosphorylation of JUN-S63, and BMS-345541 blocked it.

In some cases, such as NFKB1/p105-S903/S907, ATF2-T69/T71, and JUN-S63, BMS-345541 treatment produced a strong early inhibitory effect on phosphorylation (Fig. 2B–D). While for some phosphorylation sites, BMS-345541 treatment produced a more substantial inhibitory effect after extended treatment (3 d vs. 1 d) (Fig. 2F–I). This led us to investigate if IKK regulates TGFβ-induced EMT in a time-dependent manner. We used conducted the two-way ANOVA analysis on the phosphoproteomics data from hSAECs treated with TGFβ ± BMS-345541 for 1 d, compared to hSAECs ± BMS-345541. With this analysis, we identified 365 phosphopeptides (Supplemental Table S6) that were significantly regulated by TGFβ and BMS-345541 (two-way ANOVA TGFβ p-value <0.01, two-way ANOVA BMS p-value <0.01, and two-way ANOVA interaction p-value <0.01). A similar analysis was carried out on the phosphoproteomics data from hSAECs treated with TGFβ ± BMS-345541 for 3 d and identified 363 phosphopeptides that were significantly regulated by TGFβ and BMS-345541 after 3 d treatment (Supplemental Table S7). We carried out Panther pathway enrichment analysis on these significant phosphopeptides to identify which signaling pathways were activated by TGFβ and BMS-345541 after 1d and 3 d treatment. As shown in Fig. 2J (**left panel**), 8 IKK-dependent signaling pathways were activated after 1 d of TGFβ treatment, include TGFβ signaling pathway, Ras pathway, VEGF pathway, and inflammation-mediated by chemokine and cytokine (Supplemental Table S6). After 3 d of TGFβ treatment, 23 signaling pathways were found to be regulated by TGFβ and BMS-345541 (Fig. 2J **right panel**) (Supplemental Table S7). In addition to the 8 signaling pathways activated after 1 d of TGFβ treatment, 15 more signaling pathways were activated by TGFβ after 3 d of treatment, including Toll receptor signaling pathway, p38 MAPK pathway, and insulin/IGF pathway-mitogen activated protein kinase/MAP kinase cascade. These results indicate that IKK regulates TGFβ-induced EMT signaling pathway

in a time-dependent manner. Taken together, our study indicates that IKK regulates the phosphorylation of many proteins that are critical for TGFβ signaling, NFκB signaling, and EMT programming, suggesting that IKK is an essential mediator of the EMT process.

Next, we investigated which protein phosphorylation and signaling pathways are mediated only by TGFβ, but not by IKK. Using two-way ANOVA analysis, we identified 889 (Supplemental Table S8) and 863 phosphopeptides (Supplemental table T9) that were significantly regulated by TGFβ on day one and day three, respectively, but not affected by BMS-345541 (two-way ANOVA TGFβ p-value <0.01, two-way ANOVA BMS p-value >0.01, and two-way ANOVA interaction p-value >0.01). We found that zinc finger protein SNAI2, a transcription regulator of EMT, was phosphorylated on S87 after treatment with TGFβ for one day, and BMS-345541 did not show an inhibitory effect on this phosphorylation (Fig. 3A). Fig. 3B–E shows additional examples of phosphorylation that was regulated only by TGFβ. We carried out Panther pathway enrichment analysis on these significant phosphopeptides to identify which signaling pathways were regulated only by TGFβ but not by IKK. With this analysis, we identified nine signaling pathways regulated by TGFβ on d 1 (Supplemental Table S8) and five signaling pathways on d 3 (Supplemental Table S9), including the VEGF signaling pathway, Interleukin signaling pathway, and integrin signaling (Fig. 3F). We also identified 719 (Supplemental Table S10) and 1021 phosphorylation sites (Supplemental Table S11) regulated by IKK on d 1 and d 3, respectively, but not by TGFβ. Panther pathway enrichment analysis of 719 phosphopeptides regulated by IKK on d 1 did not yield any significant results. Panther pathway enrichment analysis of 1021 phosphorylation sites regulated by IKK on d 3 identified one significant signaling pathways: integrin signaling pathway (Supplemental Table S11).

IKKβ phosphorylates XBP1 on T48

Interestingly, in the phosphoproteomics study, we found that T48 of XBP1s was phosphorylated, as evidenced by the MS/MS spectra in Fig 4A. Additionally, in response to TGFβ stimulation, the level of phosphorylated XBP1s-T48 was increased in a time-dependent manner, and this induction was blocked by BMS-345541 (Fig. 4B). This finding prompted us to hypothesize that IKK is the kinase that directly phosphorylates XBP1s through physical interaction. To test this hypothesis, we immunoprecipitated XBP1s and measured the amount of XBP1s and IKK with SID-SRM-MS. As shown in Fig. 4C and D, the level of XBP1s was elevated after 3 d of TGFβ treatment, confirming that TGFβ activated the XBP1-UPR pathway. We found that IKKβ was co-immunoprecipitated with XBP1s, and the amount of IKKβ was increased proportionally with the level of XBP1s, indicating that IKKβ directly interacted with XBP1s. More importantly, IKKβ inhibitor blocked IKKβ-XBP1s interaction. Taken together, the data suggest that XBP1s-T48 is a substate of IKKβ, and BMS-345541 blocks this interaction and the phosphorylation of XBP1s-T48.

IKK regulates XBP1s nuclear translocation

Because the phosphorylation of T48 is required for the nuclear translocation of XBP1s[44], we examined if IKKβ regulated XBP1 nuclear translocation. We first used Western blotting to measure the level of XBP1s in the nucleus using nuclear fractionation. We found that

TGFβ treatment induced the nuclear translocation of XBP1s relative to the nuclear marker, HDAC1. Additionally we noted XBP1s nuclear translocation was blocked by BMS-345541 treatment, indicating its IKK dependence (Fig. 4E). This finding was independently vertified with SID-SRM-MS (Fig. 4F). Together, the data indicate that TGFβ-induced nuclear translocation of XBP1s is mediated by IKKβ.

IRE1-XBP1-mediated URP is activated in the early stage of EMT

Next, we examined whether the XBP1 arm of the UPR was activated at an early EMT stage. We investigated the temporal dynamics of the proteome in the early stage of TGFβ-induced EMT in the presence or absence of BMS-345541. A time-series hierarchical cluster analysis of the differentially expressed proteins using the Z-score normalized logarithmic LFQ intensity. The analysis of 2,508 significant proteins resulted in six significant clusters which mostly segregate proteins peaking on 0, 1, and 3 d of TGFβ treatment in the presence or absence of IKK inhibitor (Fig 5A), showing that TGFβ induced time-resolved changes in hSAECs proteome and many of the changes were regulated by IKK.

The GO biological process (GOBP) enrichment analysis of proteins in these clusters are shown in Supplemental Table S12. In the absence of the IKK inhibitor, the most significant GOBP enriched for the proteins peaking after 1 d of TGFβ treatment (Cluster 2) are DNA replication, translation, mRNA processing, and mRNA splicing. Cluster 3 are proteins peaking after 3 d of TGFβ, and the significantly enriched GOBP in this cluster includes biological processes related to cell shape changes such as actin-filament fragmentation and capping, and proteins targets tight junction. We also found that many biological processes involved in proteostasis are significantly enriched in this cluster. Pretreatment of hSAECs with IKK inhibitor upregulated some proteins involved in biological processes such as mitochondrial translation and mitochondrial respiratory chain. Cluster 5 and 6 are proteins peaking after 1 and 3 d of TGFβ treatment in IKK inhibitor presence, respectively. These clusters were significantly enriched for different functional annotations for processes that may be influenced by IKK mediated TGFβ signaling, including apoptosis signaling, mRNA processing, protein folding, and regulation of transcription smooth muscle cell migration.

Interestingly, bioinformatic analysis of the proteins peaked after 3 d of TGFβ treatment (Cluster 3 in Fig. 5A) found that a cluster of GOBP associated protein quality control and proteostasis was significantly enriched (fold enrichment > 5, Benjamini-Hochberg FDR <0.05) (Fig. 5B). For example, protein folding in ER, chaperone cofactor-dependent protein refolding, protein peptidyl-prolyl isomerization, IRE1-mediated unfolded protein response, UDP-N-acetylglucosamine biosynthetic process, and protein N-linked glycosylation via asparagine were all enriched. The ER stress marker, 78 kDa glucose-regulated protein (HSPA5), were upregulated after three days of TGFβ treatment (Fig. 5C). The data suggest that the cells experienced ER stress in partial EMT and activated the XBP1-UPR and protein N-glycosylation to restore the proteostasis. In our previous study of hSAECs undergoing complete mesenchymal transition (14 d TGFβ treatment), we found that the XBP1-UPR pathway was activated in response to proteotoxicity[18]. The data here suggest that the activation of the XBP1-HBP pathway occurred in complete EMT and partial EMT. hSAECs

experience ER stress as early as 3 d of TGFβ treatment and activate unfolded proteins response and protein N-glycosylation to restore the proteostasis.

We next examined if the IKK regulated the activation of XBP1-UPR in TGFβ-treated hSAECs. We conducted the two-way ANOVA analysis to identify proteins that were upregulated by TGFβ but inhibited by BMS-345541 (two-way ANOVA TGFβ p-value <0.01, two-way ANOVA BMS p-value <0.01, and two-way ANOVA interaction p-value <0.01). GOBP enrichment analysis of these proteins identified 38 enriched GO biological processes (FDR<0.05) (Supplemental Table S13), including IRE1-mediated unfolded protein response, protein folding in ER, chaperone cofactor-dependent protein refolding, regulation of ER-associated ubiquitin-dependent protein catabolic process, and ubiquitin-dependent ERAD pathway. We observed that the expression of XBP1-UPR associated genes, such as HSPA5, dynactin subunit 1 (DCNT1), and ADP-ribosylation factor GTPase-activating protein 1 (ARFGAP1) was significantly elevated after 3 d TGFβ treatment and was reduced to the basal levels by the IKK inhibitor (Fig. 5C–E). The expression of proteins involved in ERAD pathways, including heat shock protein HSP 90-beta (HSP90B1), ubiquilin-1 (UBQLNA1) and ubiquilin-2 (UBQLNA2), were induced after 3 d of TGFβ treatment, and this induction was blocked by IKK inhibitor (Fig. 5F–H). This result suggests that inhibiting IKK kinase activities reduced ER stress and attenuated the XBP1-mediated UPR and ERAD process.

XBP1-HBP-mediated glucose metabolic reprogramming is activated in the early stage of EMT

XBP1s is an upstream regulator of the HBP pathway.[18, 45] We previously reported that HBP flux and UDP-GlcNAc production were increased in hSAECs undergoing a complete mesenchymal transition (14 days TGFβ treatment). Here, we found that UDP-N-acetylglucosamine biosynthetic process and protein N-linked glycosylation via asparagine was activated as early as 3 d of TGFβ treatment (Fig. 5B). The confocal imaging of N-glycosylated proteins with lectin shows that the lectin staining in the hSAECs treated with TGFβ was significantly higher than in the untreated cells and displayed a perinuclear and cytoplasmic ER-like pattern, indicating that the abundance of intracellular glycoproteins was significantly increased in hSAECs after three days of TGFβ treatment (Fig. 6A, B). This increase of lectin staining was not observed in hSAECs treated with BMS-345541. We also observed the elevated expression of HBP enzymes, such as glucosamine 6-phosphate N-acetyltransferase (GNPNAT1), phosphoacetylglucosamine mutase (PGM3), UDP-N-acetylhexosamine pyrophosphorylase (UAP1), which was inhibited by BMS-345541 (Fig. 6C–E). Next, we measured the intracellular level of UDP-GlcNAc and found that it was upregulated after 3 d of TGFβ stimulation, and in the cells treated with BMS-345541 or, we did not observe the elevation of UDP-GlcNAc (Fig. 6F). UDP-GlcNAc is the metabolite donor of protein N-glycosylation. We found that several enzymes regulating N-linked glycosylation were significantly elevated after three days of TGFβ stimulation and restored to the untreated level by IKK inhibitor (Fig. 6G–I). Collectively, these data suggest that TGFβ induced the activation of the XBP1-HBP pathway and led to glucose metabolic reprogramming in the early stage of EMT, and this biological process was IKK-dependent.

DISCUSSION

IKK-NFκB signaling is central to the pathophysiology of airway inflammation. Chronic exposure to environmental stimuli, such as aeroallergens and viruses, induces innate inflammation in the airway through IKK-NFκB signaling, followed by a profibrogenic EMT process in primary human small airway epithelial cells[7]. Studies on various airway remodeling mouse models confirm EMT plays pathological roles in barrier disruption, ECM deposition, and airway remodeling.[5–7] The finding that EMT is produced in a variety of airway diseases, including virus-induced inflammation[5], COPD[46–48], and allergic airway disease[7, 10], indicates that this is a common pathogenic response to airway injury.

EMT involves a series of cell-state changes driven by core mesenchymal regulatory factors, including SNAI1/2 and ZEB1.[11–14] We previously reported that IKK-NFκB signaling is one of the signaling cassettes that are activated in the early stage of EMT and is required for the expression of SNAIs and ZEBs, and is a driver of the pathological airway mucosa changes associated with epithelial de-differentiation and mesenchymal transition.[5–7, 16, 25] We employed a time-series phosphoproteomics approach and a highly specific IKK inhibitor to characterize how IKK, a critical serine/threonine kinase of IKK-NFκB signaling, regulated early EMT signaling events in hSAECs. This analysis identified 24 IKK-mediated EMT signaling pathways early in EMT, suggesting that IKK plays profound regulatory roles in the EMT process. As expected, the inflammation mediated by chemokine and cytokine is one of the early IKK-mediated signaling pathways that were activated on the first day of TGFβ treatment. Notably, we observed robust induced phosphorylation of NFKB1-S903/S907 by TGFβ, and this induction was abolished by IKK inhibitor. NFKB1/p105 is a subunit of the NFκB transcription complex. It functions as a cytoplasmic inhibitor for NFκB, and the proteolytic processing of its inhibitory C-terminal region is required for the generation of active NFκB complex.[17] Phosphorylation at S903 and S907 primes NFKB1/p105 for proteolytic processing in response to TNFα stimulation[49–50], and the mutations of S903 and S907 to alanine prevent p105 proteolysis in response to TNFα. We are the first to report that these two sites were phosphorylated in response to TGFβ. We previously revealed that IκB-NFκB is a controller of EMT because the mesenchymal transition was prevented by administering a small-molecule IKK inhibitor, BMS-345541.[5, 16] Here, we propose a mechanism by which IKKs-NFκB regulates EMT through IKK-mediated phosphorylation of NFKB1-S903/S907, which primes the proteolysis of NFKB1/p105, releases cytoplasmic RelA, and facilitates the formation of active p65-p50 complex and its nuclear translocation.

TGFβ signaling pathway and p38 MAPK signaling pathway are more substantially activated after 3 d of TGFβ stimulation than 1 d of TGFβ treatment. Although TGFβ-stimulated activation of ATF2, JUN, and p38 MAPK activity has been demonstrated previously in different cell types[40–43, 51], we show that BMS-345541 inhibited the TGFβ induced phosphorylation of ATF2-T69/T71, JUN-S63, MAPK1-T185/Y187, and MAPK3-T202/Y204. Phosphorylation of JUN-S63 and ATF2-T69/T71 is required for its transcription activities, and phosphorylation of MAPK1-T185/Tyr187 and MAPK3-T202/Y204 is essential for their kinase activity.

Our study provides another layer of evidence that IKK-NFκB signaling is a central regulator of EMT. In previous studies, we revealed that NFκB/RelA directly regulates core mesenchymal transcription factors through bromodomain recruitment, enhancing transcriptional elongation.[5, 7, 14, 16, 23, 25] The phosphoproteomics study here is the first to report that IKK regulates TGFβ-induced phosphorylation of ATF2, JUN, and NFκB1 transcription factors independently of gene expression activation.

We also identified many TGFβ-stimulated phosphorylated sites that were not regulated by IKK. For example, SNAI2, a transcription regulator of EMT, was phosphorylated on S87 in response to TGFβ. Phosphorylation of SNAI2-S87 regulates the expression of vimentin, a marker of EMT.[53] BMS-345541 did not affect the phosphorylation of SNAI2-S87. Analysis of amino acid residues surrounding S87 matches the phosphorylation consensus motifs of ERK (P-X-S/T-P), suggesting that SNAI2-S87 was likely phosphorylated by ERK, not by IKK. Overall, our quantitative phosphoproteomics study revealed that TGFβ induces wide-range, time-resolved phosphorylation in both IKK-dependent and independent manner.

IKK-NFκB signaling mediated glucose metabolic reprogramming in the early stage of EMT is another important finding of our study. Epithelial cells produce few ECM proteins under normal conditions but dramatically enhance FN1 and collagen production in EMT, resulting in proteotoxicity. We recently revealed a new molecular mechanism underlying the transformation of the protein factory and secretory machinery during the mesenchymal transition.[18] We found that hSAECs undergoing a complete EMT (14 d of TGFβ treatment) activate the XBP1-axis of UPR to deal with the ER stress caused by the increased demand for ECM protein synthesis. XBP1s initiates transcriptional programs that upregulate a broad spectrum of UPR-associated genes involved in protein entry into the ER, protein folding, ERAD, and ER biogenesis. Furthermore, our work reveals another critical function of XBP1-URP. We found that mesenchymal transition in hSAECs reprograms glucose metabolism to HBP via XBP1-mediated UPR[18], shifting the glucose flux from glycolysis to the production of uridine diphosphate N-acetylglucosamine (UDP-GlcNAc). The accumulation of intracellular UDP-GlcNAc increases the protein N-glycosylation of ECM (N-matrisome), which reduces proteotoxic stress by increasing the folding of insoluble ECM components.[18] Our earlier study was not designed to identify the temporal activation of the UPR-HBP program.

In this study, we found that TGFβ-stimulated XBP1-HBP pathway activation also occurred early in EMT when cells are in partial EMT state coinciding with substantial expression of ECM components. These data suggest that the XBP1-HBP pathway is an adaptive response activated early during the EMT process. More importantly, we found that TGFβ-induced activation of IKK-NFκB signaling preceded the XBP1-HBP pathway, and the activation of the XBP1-HBP pathway is IKKβ-dependent. We show that IKKβ directly phosphorylates the T48 residue of XBP1s and mediates the nuclear translocation of XBP1s. Liu et al. also reported that IKKβ increases the activity and stability of XBP1s in hepatocytes through phosphorylation of XBP1s.[44] Our studies extend these findings by discovering that XBP1-HBP mediated protein folding, ERAD, ER biogenesis, and protein N-glycosylation were IKK regulated, demonstrating IKK is a major upstream regulator of XBP-HBP-mediated glucose metabolic reprogramming and proteostasis.

We propose a novel mechanism that links inflammation with proteostasis in mesenchymal cells. As schematically diagramed in Fig. 7, In response to TGFβ stimulation, IKKβ mediates the activation of EMT signaling pathways and initiates the EMT process, which induces the gene expression of ECM proteins. Excessive production of ECM proteins induces ER stress and increases the alternative splicing of XBP1s. IKKβ directly phosphorylates XBP1s and increases its nuclear translocation and stability. Consequentially, XBP1s activates UPR- and ERAD-associated genes and genes regulating HBP, increasing ER folding capacity, HBP flux, and protein N-glycosylation, restoring the proteostasis. It was previously reported that the NFκB pathway regulates protein aggregate clearance and proteostasis by modulating autophagic activity.[54–55] We revealed a new role of IKK-NFκB signaling in regulating proteostasis via IKKβ-XBP1-HBP mediated unfolded protein response and glucose metabolic reprogramming.

Our study here presents a new mechanism for the pathogenesis of airway remodeling diseases, where inflammation plays a pro-survival role in epithelial cells undergoing EMT by activating the IKKβ-XBP1-HBP pathway. The injuries to lung epithelium induce innate immune response through IKK-NFκB signaling, which controls the expression of core transcription regulators of EMT and also regulates many EMT signaling pathways through IKK-mediated protein phosphorylation. In addition, IKKβ phosphorylates XBP1s and increases XBP1s nuclear translocation, activating UPR, expanding the ER capacity and secretory machinery, and upregulating ERAD. Activation of IKKβ-XBP1 also increases the HBP flux and the expression of the enzymes regulating protein N-glycosylation, promoting the secretion of ECM proteins and leading to ECM accumulation and airway remodeling. Our study suggests that targeting IKK-NFκB signaling and the XBP1-HBP pathway may provide a practical therapeutic approach for airway remodeling.

Supplementary Material

Refer to Web version on PubMed Central for supplementary material.

Acknowledgments

This work was supported by the National Institutes of Health Grants NIAID 1R21AI133454 (to YXZ, ARB).

Abbreviations:

AGC	Automatic gain control
ANOVA	Analysis of variance
BCA	bicinchoninic acid
ECM	Extracellular matrix
ER	endoplasmic reticulum
ERAD	ER-associated protein degradation
FDR	False discovery rate

GO	Gene ontolog
GOBP	Gene ontology biological process
HBP	Hexosamine biosynthesis pathway
HCD	High energy collisional dissociation
LC	Liquid chromatography
MMP	Metalloproteinases
MS	Mass spectrometry
PCA	Principle component analysis
PDI	protein disulfide isomerase
PTM	Post-translational modifications
Q	Quadrupole
Q-RT-PCR	Quantitative real-time reverse transcription-PCR
SCX	Strong cation exchange
SID	Stable isotope dilution
SIS	Stable isotope labeled internal standard
SRM	Selected reaction monitoring
TGF	Transforming growth factor
TM	Tunicamycin
UDP-GlcNAc	Uradine diphosphate-N-acetyl-glucosamine
UHPLC	Ultra high performance liquid chromatography
UPR	Unfolded protein response

References

1. Brasier AR, Mechanisms how mucosal innate immunity affects progression of allergic airway disease. Expert Rev Respir Med 2019, 13 (4), 349–356. [PubMed: 30712413]
2. Elias JA; Zhu Z; Chupp G; Homer RJ, Airway remodeling in asthma. J Clin Invest 1999, 104 (8), 1001–6. [PubMed: 10525034]
3. Fanta CH, Asthma. N Engl J Med 2009, 360 (10), 1002–14. [PubMed: 19264689]
4. Hammad H; Lambrecht BN, Dendritic cells and epithelial cells: linking innate and adaptive immunity in asthma. Nat Rev Immunol 2008, 8 (3), 193–204. [PubMed: 18301423]
5. Tian B; Patrikeev I; Ochoa L; Vargas G; Belanger KK; Litvinov J; Boldogh I; Ameredes BT; Motamedi M; Brasier AR, NF-kappaB Mediates Mesenchymal Transition, Remodeling, and Pulmonary Fibrosis in Response to Chronic Inflammation by Viral RNA Patterns. Am J Respir Cell Mol Biol 2017, 56 (4), 506–520. [PubMed: 27911568]

6. Graber TG; Rawls BL; Tian B; Durham WJ; Brightwell CR; Brasier AR; Rasmussen BB; Fry CS, Repetitive TLR3 activation in the lung induces skeletal muscle adaptations and cachexia. Exp Gerontol 2018, 106, 88–100. [PubMed: 29452288]
7. Tian B; Hosoki K; Liu Z; Yang J; Zhao Y; Sun H; Zhou J; Rytting E; Kaphalia L; Calhoun WJ; Sur S; Brasier AR, Mucosal bromodomain-containing protein 4 mediates aeroallergen-induced inflammation and remodeling. J Allergy Clin Immunol 2019, 143 (4), 1380–1394 e9. [PubMed: 30321559]
8. Holgate ST; Lackie PM; Howarth PH; Roche WR; Puddicombe SM; Richter A; Wilson SJ; Holloway JW; Davies DE, Invited lecture: activation of the epithelial mesenchymal trophic unit in the pathogenesis of asthma. Int Arch Allergy Immunol 2001, 124 (1–3), 253–8. [PubMed: 11306984]
9. Holgate ST, Epithelium dysfunction in asthma. J Allergy Clin Immunol 2007, 120 (6), 1233–44; quiz 1245–6. [PubMed: 18073119]
10. Sagara H; Okada T; Okumura K; Ogawa H; Ra C; Fukuda T; Nakao A, Activation of TGF-beta/Smad2 signaling is associated with airway remodeling in asthma. J Allergy Clin Immunol 2002, 110 (2), 249–54. [PubMed: 12170265]
11. Zhang J; Tian XJ; Zhang H; Teng Y; Li R; Bai F; Elankumaran S; Xing J, TGF-beta-induced epithelial-to-mesenchymal transition proceeds through stepwise activation of multiple feedback loops. Sci Signal 2014, 7 (345), ra91.
12. Kalluri R; Neilson EG, Epithelial-mesenchymal transition and its implications for fibrosis. J Clin Invest 2003, 112 (12), 1776–84. [PubMed: 14679171]
13. Kalluri R; Weinberg RA, The basics of epithelial-mesenchymal transition. J Clin Invest 2009, 119 (6), 1420–8. [PubMed: 19487818]
14. Lamouille S; Xu J; Derynck R, Molecular mechanisms of epithelial-mesenchymal transition. Nat Rev Mol Cell Biol 2014, 15 (3), 178–96. [PubMed: 24556840]
15. Tian B; Nowak DE; Brasier AR, A TNF-induced gene expression program under oscillatory NF-kappaB control. BMC Genomics 2005, 6, 137. [PubMed: 16191192]
16. Tian B; Widen SG; Yang J; Wood TG; Kudlicki A; Zhao Y; Brasier AR, The NFkappaB subunit RELA is a master transcriptional regulator of the committed epithelial-mesenchymal transition in airway epithelial cells. J Biol Chem 2018, 293 (42), 16528–16545. [PubMed: 30166344]
17. Brasier AR, The NF-kappaB regulatory network. Cardiovasc Toxicol 2006, 6 (2), 111–30. [PubMed: 17303919]
18. Zhang J; Jamaluddin M; Zhang Y; Widen SG; Sun H; Brasier AR; Zhao Y, Type II Epithelial-Mesenchymal Transition Upregulates Protein N-Glycosylation To Maintain Proteostasis and Extracellular Matrix Production. J Proteome Res 2019, 18 (9), 3447–3460. [PubMed: 31424945]
19. Johnson PR; Burgess JK; Underwood PA; Au W; Poniris MH; Tamm M; Ge Q; Roth M; Black JL, Extracellular matrix proteins modulate asthmatic airway smooth muscle cell proliferation via an autocrine mechanism. J Allergy Clin Immunol 2004, 113 (4), 690–6. [PubMed: 15100675]
20. Yick CY; Ferreira DS; Annoni R; von der Thusen JH; Kunst PW; Bel EH; Lutter R; Mauad T; Sterk PJ, Extracellular matrix in airway smooth muscle is associated with dynamics of airway function in asthma. Allergy 2012, 67 (4), 552–9. [PubMed: 22229658]
21. Araujo BB; Dolhnikoff M; Silva LF; Elliot J; Lindeman JH; Ferreira DS; Mulder A; Gomes HA; Fernezlian SM; James A; Mauad T, Extracellular matrix components and regulators in the airway smooth muscle in asthma. Eur Respir J 2008, 32 (1), 61–9. [PubMed: 18321931]
22. Agache I; Akdis C; Jutel M; Virchow JC, Untangling asthma phenotypes and endotypes. Allergy 2012, 67 (7), 835–46. [PubMed: 22594878]
23. Tian B; Liu Z; Litvinov J; Maroto R; Jamaluddin M; Rytting E; Patrikeev I; Ochoa L; Vargas G; Motamedi M; Ameredes BT; Zhou J; Brasier AR, Efficacy of Novel Highly Specific Bromodomain-Containing Protein 4 Inhibitors in Innate Inflammation-Driven Airway Remodeling. Am J Respir Cell Mol Biol 2019, 60 (1), 68–83. [PubMed: 30153047]
24. Yang J; Tian B; Sun H; Garofalo RP; Brasier AR, Epigenetic silencing of IRF1 dysregulates type III interferon responses to respiratory virus infection in epithelial to mesenchymal transition. Nat Microbiol 2017, 2, 17086. [PubMed: 28581456]

25. Tian B; Li X; Kalita M; Widen SG; Yang J; Bhavnani SK; Dang B; Kudlicki A; Sinha M; Kong F; Wood TG; Luxon BA; Brasier AR, Analysis of the TGFbeta-induced program in primary airway epithelial cells shows essential role of NF-kappaB/RelA signaling network in type II epithelial mesenchymal transition. BMC Genomics 2015, 16, 529. [PubMed: 26187636]
26. Zhao Y; Tian B; Sadygov RG; Zhang Y; Brasier AR, Integrative proteomic analysis reveals reprograming tumor necrosis factor signaling in epithelial mesenchymal transition. J Proteomics 2016, 148, 126–38. [PubMed: 27461979]
27. Idris AI; Krishnan M; Simic P; Landao-Bassonga E; Mollat P; Vukicevic S; Ralston SH, Small molecule inhibitors of IkappaB kinase signaling inhibit osteoclast formation in vitro and prevent ovariectomy-induced bone loss in vivo. FASEB J 2010, 24 (11), 4545–55. [PubMed: 20647545]
28. Zakaria N; Mohd Yusoff N; Zakaria Z; Widera D; Yahaya BH, Inhibition of NF-kappaB Signaling Reduces the Stemness Characteristics of Lung Cancer Stem Cells. Front Oncol 2018, 8, 166. [PubMed: 29868483]
29. Du Z; Whitt MA; Baumann J; Garner JM; Morton CL; Davidoff AM; Pfeffer LM, Inhibition of type I interferon-mediated antiviral action in human glioma cells by the IKK inhibitors BMS-345541 and TPCA-1. J Interferon Cytokine Res 2012, 32 (8), 368–77. [PubMed: 22509977]
30. Sasai K; Ikeda Y; Fujii T; Tsuda T; Taniguchi N, UDP-GlcNAc concentration is an important factor in the biosynthesis of beta1,6-branched oligosaccharides: regulation based on the kinetic properties of N-acetylglucosaminyltransferase V. Glycobiology 2002, 12 (2), 119–27. [PubMed: 11886845]
31. Cox J; Mann M, MaxQuant enables high peptide identification rates, individualized p.p.b.-range mass accuracies and proteome-wide protein quantification. Nat Biotechnol 2008, 26 (12), 1367–72. [PubMed: 19029910]
32. Cox J; Hein MY; Luber CA; Paron I; Nagaraj N; Mann M, Accurate proteome-wide label-free quantification by delayed normalization and maximal peptide ratio extraction, termed MaxLFQ. Molecular & cellular proteomics : MCP 2014, 13 (9), 2513–26. [PubMed: 24942700]
33. Tyanova S; Temu T; Sinitcyn P; Carlson A; Hein MY; Geiger T; Mann M; Cox J, The Perseus computational platform for comprehensive analysis of (prote)omics data. Nat Methods 2016, 13 (9), 731–40. [PubMed: 27348712]
34. Gaudet P; Livstone MS; Lewis SE; Thomas PD, Phylogenetic-based propagation of functional annotations within the Gene Ontology consortium. Brief Bioinform 2011, 12 (5), 449–62. [PubMed: 21873635]
35. Zhao Y; Brasier AR, Applications of selected reaction monitoring (SRM)-mass spectrometry (MS) for quantitative measurement of signaling pathways. Methods 2013, 61 (3), 313–22. [PubMed: 23410677]
36. Vizcaino JA; Deutsch EW; Wang R; Csordas A; Reisinger F; Rios D; Dianes JA; Sun Z; Farrah T; Bandeira N; Binz PA; Xenarios I; Eisenacher M; Mayer G; Gatto L; Campos A; Chalkley RJ; Kraus HJ; Albar JP; Martinez-Bartolome S; Apweiler R; Omenn GS; Martens L; Jones AR; Hermjakob H, ProteomeXchange provides globally coordinated proteomics data submission and dissemination. Nature biotechnology 2014, 32 (3), 223–6.
37. Burke JR; Pattoli MA; Gregor KR; Brassil PJ; MacMaster JF; McIntyre KW; Yang X; Iotzova VS; Clarke W; Strnad J; Qiu Y; Zusi FC, BMS-345541 is a highly selective inhibitor of I kappa B kinase that binds at an allosteric site of the enzyme and blocks NF-kappa B-dependent transcription in mice. J Biol Chem 2003, 278 (3), 1450–6. [PubMed: 12403772]
38. Salmeron A; Janzen J; Soneji Y; Bump N; Kamens J; Allen H; Ley SC, Direct phosphorylation of NF-kappaB1 p105 by the IkappaB kinase complex on serine 927 is essential for signal-induced p105 proteolysis. J Biol Chem 2001, 276 (25), 22215–22. [PubMed: 11297557]
39. Heissmeyer V; Krappmann D; Wulczyn FG; Scheidereit C, NF-kappaB p105 is a target of IkappaB kinases and controls signal induction of Bcl-3-p50 complexes. EMBO J 1999, 18 (17), 4766–78. [PubMed: 10469655]
40. Venkov C; Plieth D; Ni T; Karmaker A; Bian A; George AL Jr.; Neilson EG, Transcriptional networks in epithelial-mesenchymal transition. PLoS One 2011, 6 (9), e25354. [PubMed: 21980432]

41. Sano Y; Harada J; Tashiro S; Gotoh-Mandeville R; Maekawa T; Ishii S, ATF-2 is a common nuclear target of Smad and TAK1 pathways in transforming growth factor-beta signaling. J Biol Chem 1999, 274 (13), 8949–57. [PubMed: 10085140]
42. Fuchs SY; Tappin I; Ronai Z, Stability of the ATF2 transcription factor is regulated by phosphorylation and dephosphorylation. J Biol Chem 2000, 275 (17), 12560–4. [PubMed: 10777545]
43. Smeal T; Binetruy B; Mercola DA; Birrer M; Karin M, Oncogenic and transcriptional cooperation with Ha-Ras requires phosphorylation of c-Jun on serines 63 and 73. Nature 1991, 354 (6353), 494–6. [PubMed: 1749429]
44. Liu J; Ibi D; Taniguchi K; Lee J; Herrema H; Akosman B; Mucka P; Salazar Hernandez MA; Uyar MF; Park SW; Karin M; Ozcan U, Inflammation Improves Glucose Homeostasis through IKKbeta-XBP1s Interaction. Cell 2016, 167 (4), 1052–1066 e18. [PubMed: 27814504]
45. Wang ZV; Deng Y; Gao N; Pedrozo Z; Li DL; Morales CR; Criollo A; Luo X; Tan W; Jiang N; Lehrman MA; Rothermel BA; Lee AH; Lavandero S; Mammen PPA; Ferdous A; Gillette TG; Scherer PE; Hill JA, Spliced X-box binding protein 1 couples the unfolded protein response to hexosamine biosynthetic pathway. Cell 2014, 156 (6), 1179–1192. [PubMed: 24630721]
46. Jolly MK; Ward C; Eapen MS; Myers S; Hallgren O; Levine H; Sohal SS, Epithelial-mesenchymal transition, a spectrum of states: Role in lung development, homeostasis, and disease. Dev Dyn 2018, 247 (3), 346–358. [PubMed: 28646553]
47. Eapen MS; Hansbro PM; Larsson-Callerfelt AK; Jolly MK; Myers S; Sharma P; Jones B; Rahman MA; Markos J; Chia C; Larby J; Haug G; Hardikar A; Weber HC; Mabeza G; Cavalheri V; Khor YH; McDonald CF; Sohal SS, Chronic Obstructive Pulmonary Disease and Lung Cancer: Underlying Pathophysiology and New Therapeutic Modalities. Drugs 2018, 78 (16), 1717–1740. [PubMed: 30392114]
48. Sohal SS, Epithelial and endothelial cell plasticity in chronic obstructive pulmonary disease (COPD). Respir Investig 2017, 55 (2), 104–113.
49. Demarchi F; Bertoli C; Sandy P; Schneider C, Glycogen synthase kinase-3 beta regulates NF-kappa B1/p105 stability. J Biol Chem 2003, 278 (41), 39583–90. [PubMed: 12871932]
50. Fujimoto K; Yasuda H; Sato Y; Yamamoto K, A role for phosphorylation in the proteolytic processing of the human NF-kappa B1 precursor. Gene 1995, 165 (2), 183–9. [PubMed: 8522173]
51. Bakin AV; Rinehart C; Tomlinson AK; Arteaga CL, p38 mitogen-activated protein kinase is required for TGFbeta-mediated fibroblastic transdifferentiation and cell migration. J Cell Sci 2002, 115 (Pt 15), 3193–206. [PubMed: 12118074]
52. Chang H; Liu Y; Xue M; Liu H; Du S; Zhang L; Wang P, Synergistic action of master transcription factors controls epithelial-to-mesenchymal transition. Nucleic Acids Res 2016, 44 (6), 2514–27. [PubMed: 26926107]
53. Virtakoivu R; Mai A; Mattila E; De Franceschi N; Imanishi SY; Corthals G; Kaukonen R; Saari M; Cheng F; Torvaldson E; Kosma VM; Mannermaa A; Muharram G; Gilles C; Eriksson J; Soini Y; Lorens JB; Ivaska J, Vimentin-ERK Signaling Uncouples Slug Gene Regulatory Function. Cancer Res 2015, 75 (11), 2349–62. [PubMed: 25855378]
54. Mukherjee A; Hidvegi T; Araya P; Ewing M; Stolz DB; Perlmutter DH, NFkappaB mitigates the pathological effects of misfolded alpha1-antitrypsin by activating autophagy and an integrated program of proteostasis mechanisms. Cell Death Differ 2019, 26 (3), 455–469. [PubMed: 29795336]
55. Nivon M; Fort L; Muller P; Richet E; Simon S; Guey B; Fournier M; Arrigo AP; Hetz C; Atkin JD; Kretz-Remy C, NFkappaB is a central regulator of protein quality control in response to protein aggregation stresses via autophagy modulation. Mol Biol Cell 2016, 27 (11), 1712–27. [PubMed: 27075172]

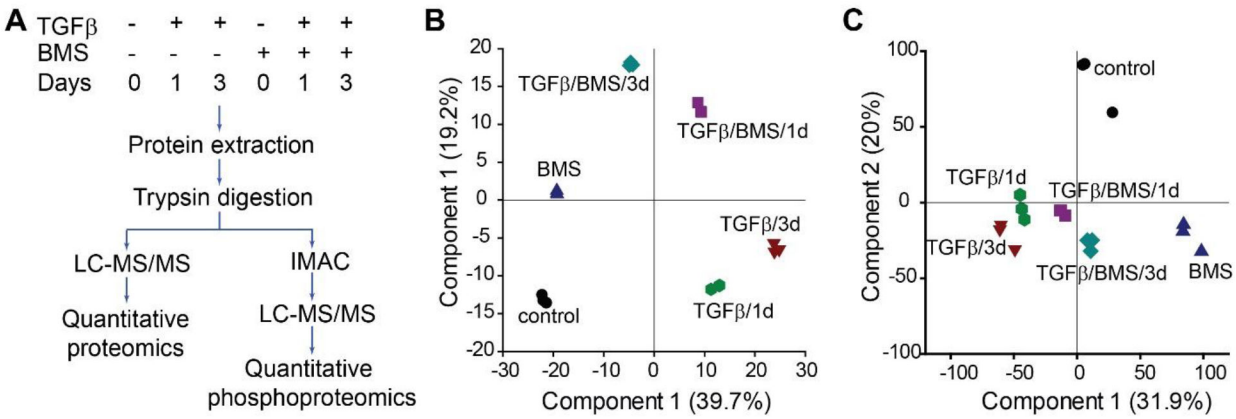

Figure 1. Proteomics and phosphoproteomics of early EMT signaling in the presence or absence IKK inhibitor, BMS-345541.

(A) Experimental design and identification strategy. hSAECs treated with TGFβ for 0, 1, and 3 d in the presence or absence IKK inhibitor, BMS-345541. Each experiment group has three biological replicates. (B) Principal component analysis (PCA) of significant proteins (multiple sample ANOVA, Permutation-based FDR 1%). (C) PCA of significant phosphopeptides (multiple sample ANOVA, Permutation-based FDR 1%).

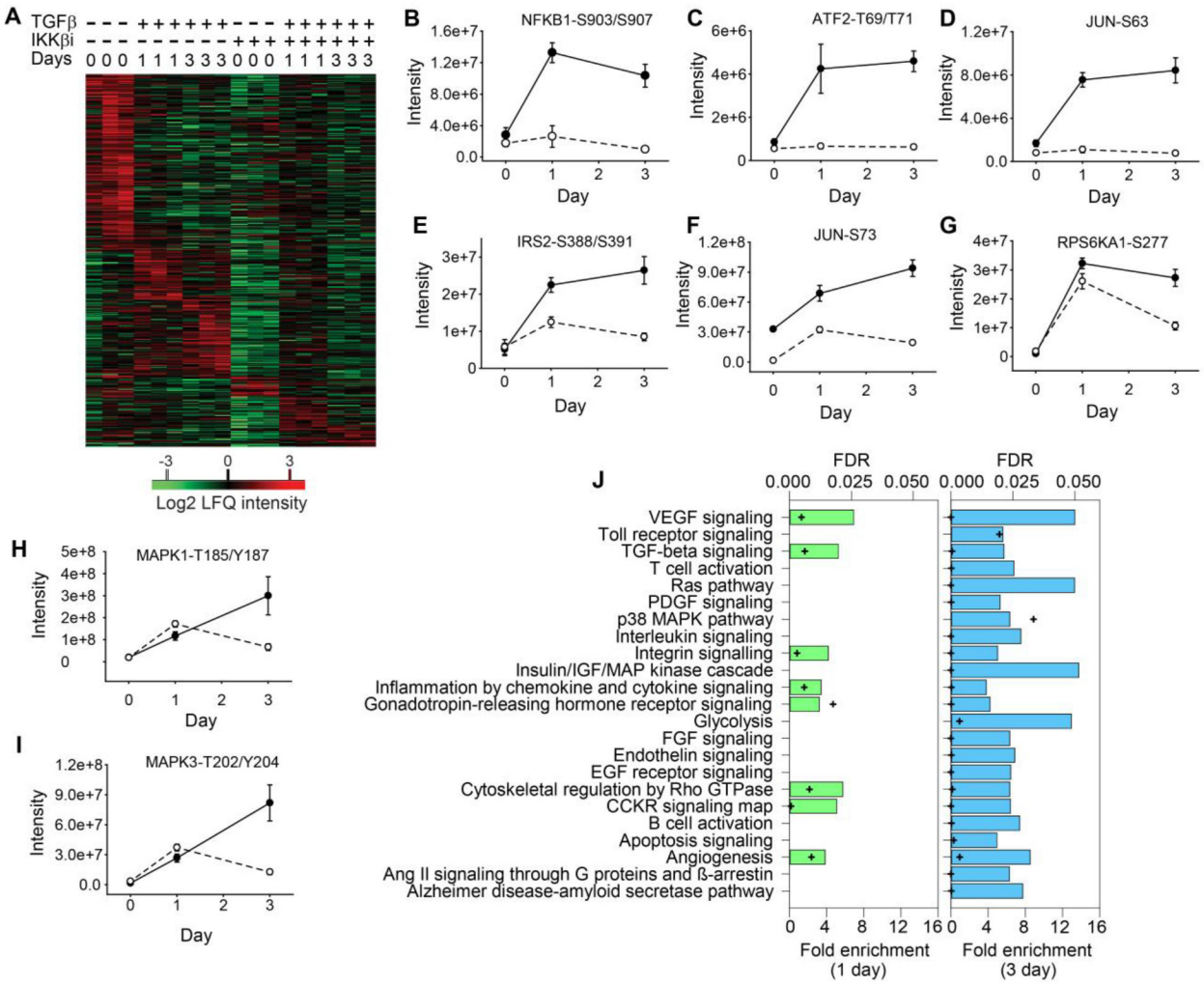

Figure 2. TGFβ- and IKK-mediated protein phosphorylation.

(A) Time-series phosphoproteomics of hSAECs in response to TGFβ stimulation in the presence or absence of BMS-345541. (B)-(I) Time-series profile of phosphorylated NFKB1-S903/S907, ATF2-T51, JUN-S63, IRS2-S388/S391, JUN-S73, RPS6KA4-T681, RPS6KA1-S277, and MAPK3-T202/Y204. The solid circle and line is the time-series profile of phosphopeptides in the absence of IKK inhibitor; the open circle and dot line is the time-series profile of phosphopeptides in the presence of IKK inhibitor; error bar, standard error. (J) Panther signaling pathways regulated by both TGFβ and IKK. Green bar, signaling pathways activated in day 1; blue bars, signaling pathways activated in day 3; +, significance level of enrichment analysis (FDR corrected p-value).

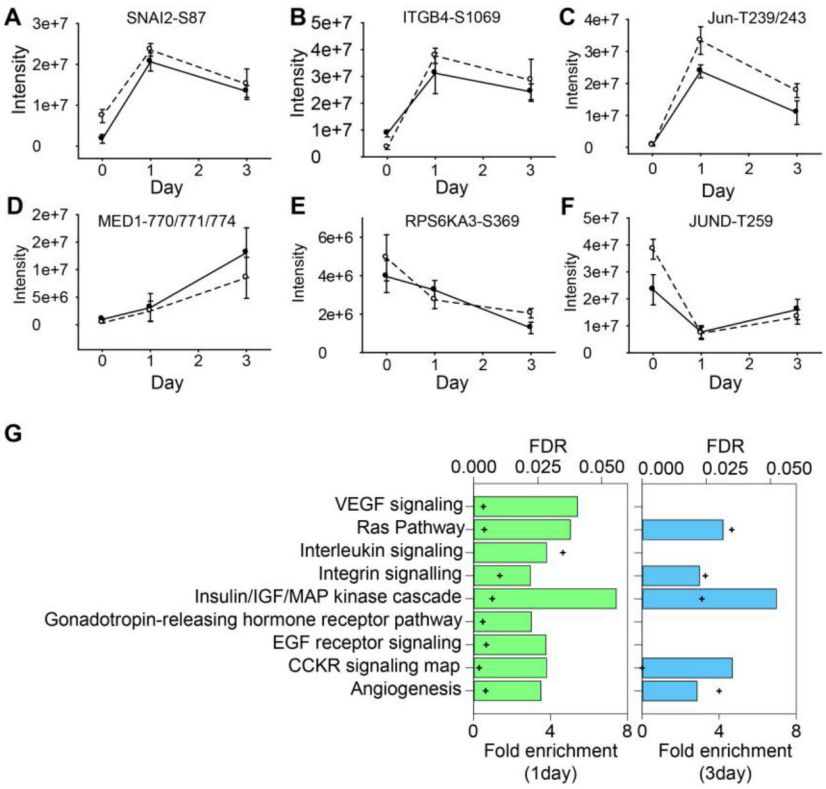

Figure 3. IKK-independent protein phosphorylation in the early stage of EMT.

(A)-(F) Time-series profile of phosphorylated SNAI2-S87, ITGB4-S1069, JUN-T239/S243, MED1-S770/S771/S774, RPS6KA3-S369, and JUND-T259. The solid circle and line is the time-series profile of phosphopeptides in the absence of IKK inhibitor; the open circle and dot line is the time-series profile of phosphopeptides in the presence of IKK inhibitor; error bar, standard error. (G) Panther signaling pathways activated by TGFβ in an IKK-independent manner. Green bar, signaling pathways activated in day 1; blue bars, signaling pathways activatied in day 3; +, significance level of enrichment analysis (FDR corrected p-value).

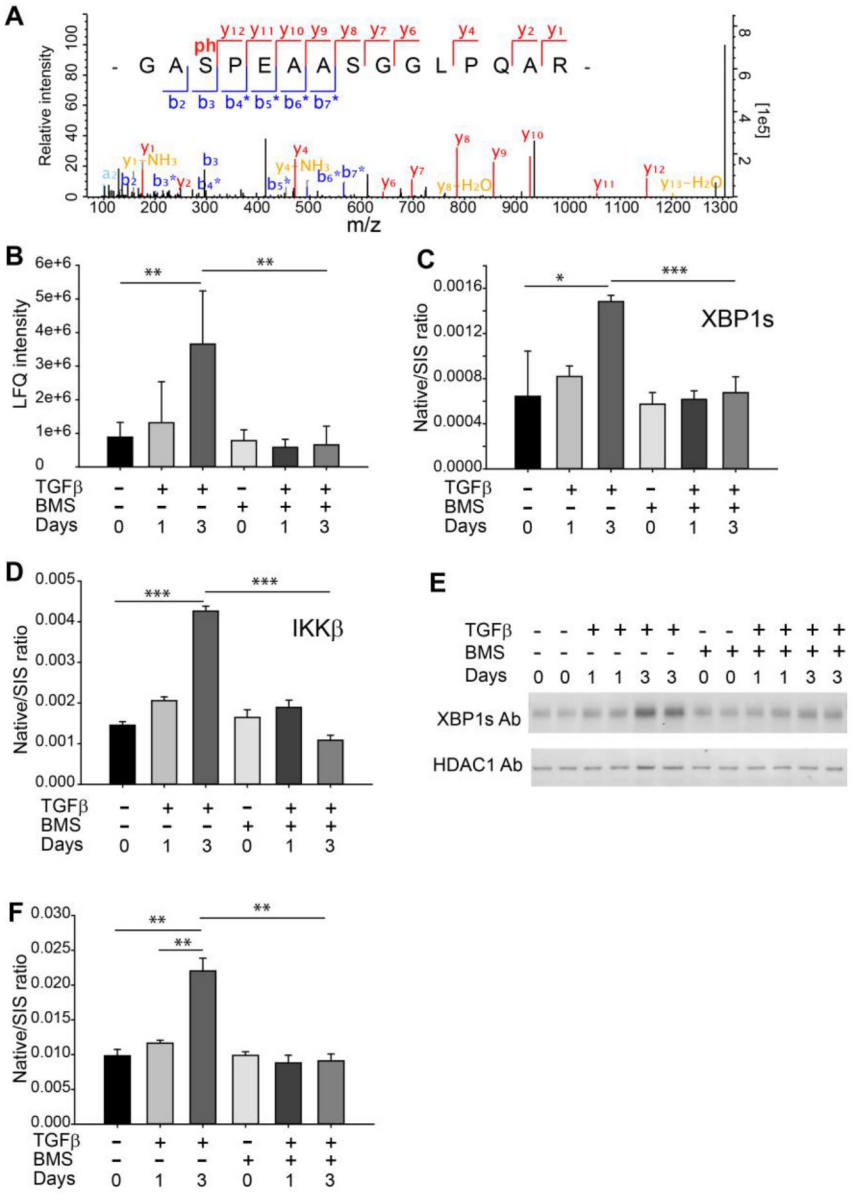

Figure 4. IKKβ phosphorylates XBP1s-T48 and regulates XBP1-mediated UPR.

The hSAECs were treated with TGFβ for 1 and 3 d in the presence or absence of BMS-345541. (A) MS/MS spectrum of phosphorylation of XBP1s-T48. (B) The level of phosphorylated XBP1s-T48. (C) and (D) IP-SRM analysis of of XBP1s and IKKβ. The XBP1-IKKβ was immunoprecipitated using XBP1 antibody, and the level of XBP1s and IKKβ were measured with SID-SRM-MS. (E) Western blot of XBP1s in the nucleus. Nuclear fractions were prepared. Lower band, HDAC1 staining demonstrates equivalent abundance of nuclear proteins in each lane. (F) SRM measurement of nuclear XBP1s. t-test p-value: *, $p<0.05$; **, $p<0.01$; ***, $p<0.001$. Native/SIS ratio, SRM intensity of native peptide derived from sample/SRM intensity of stable-isotope labeled peptide.

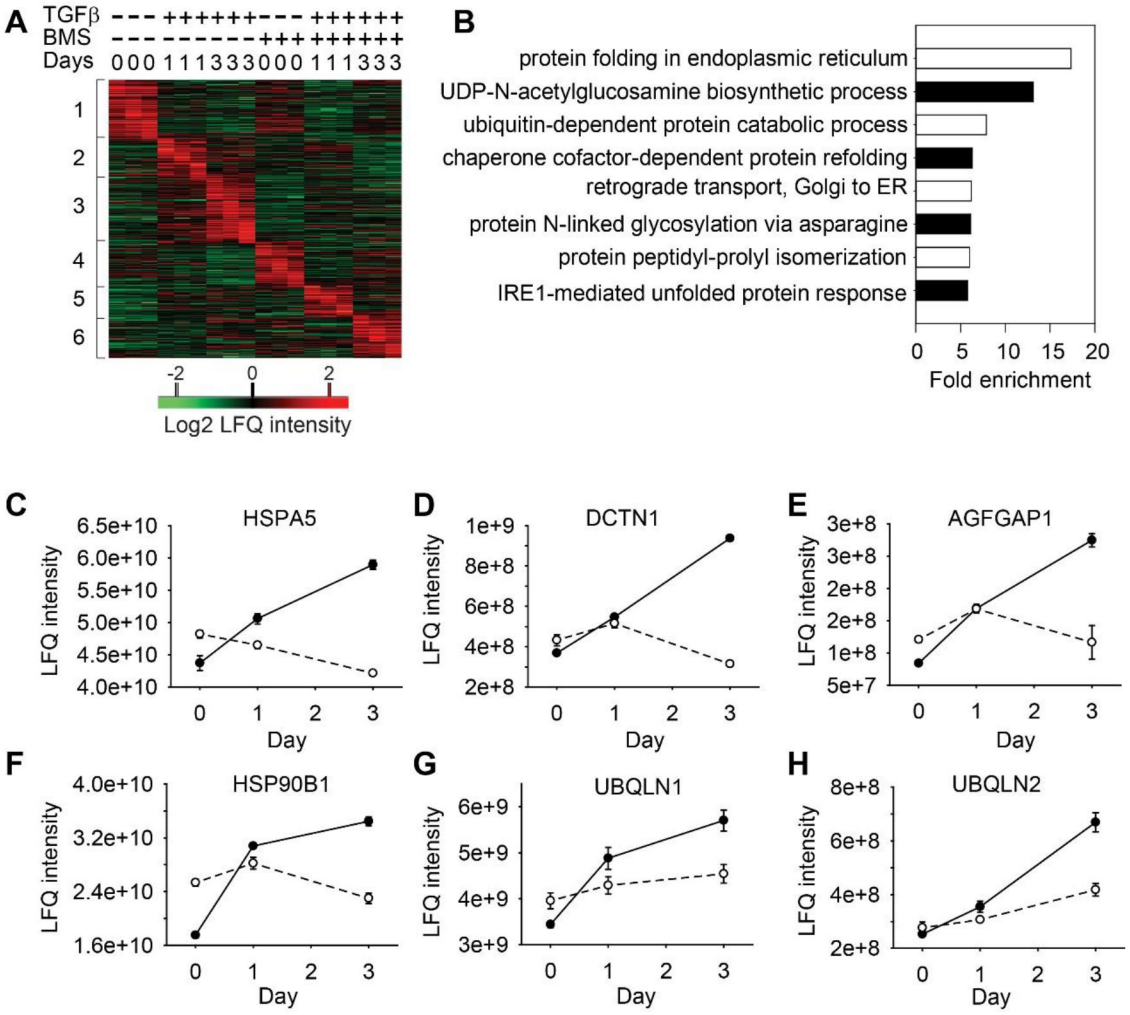

Figure 5. TGFβ- and IKK-mediated protein profiles.

(A) Time-series proteomics of hSAECs in response to TGFβ stimulation in the presence or absence of IKK inhibitor. (B) GOBP annotation enrichment of proteins that were upregulated after 3 d of TGFβ treatment and blocked by BMS-345541 (the proteins in Cluster 3 in Fig. 5A; and only UPR and HBP related annotations are shown, the full list of GO annotation are listed in Supplemental Table S11). (C)-(E) Time-series protein profiles of some IRE1-XBP1 mediated genes. The solid circle and line, the time-series profile of phosphopeptides in the absence of IKK inhibitor; the open circle and dot line, the time-series profile of phosphopeptides in the presence of IKK inhibitor; error bar, standard error. (F)-(H) Time-series protein profiles of some genes involved in ERAD.

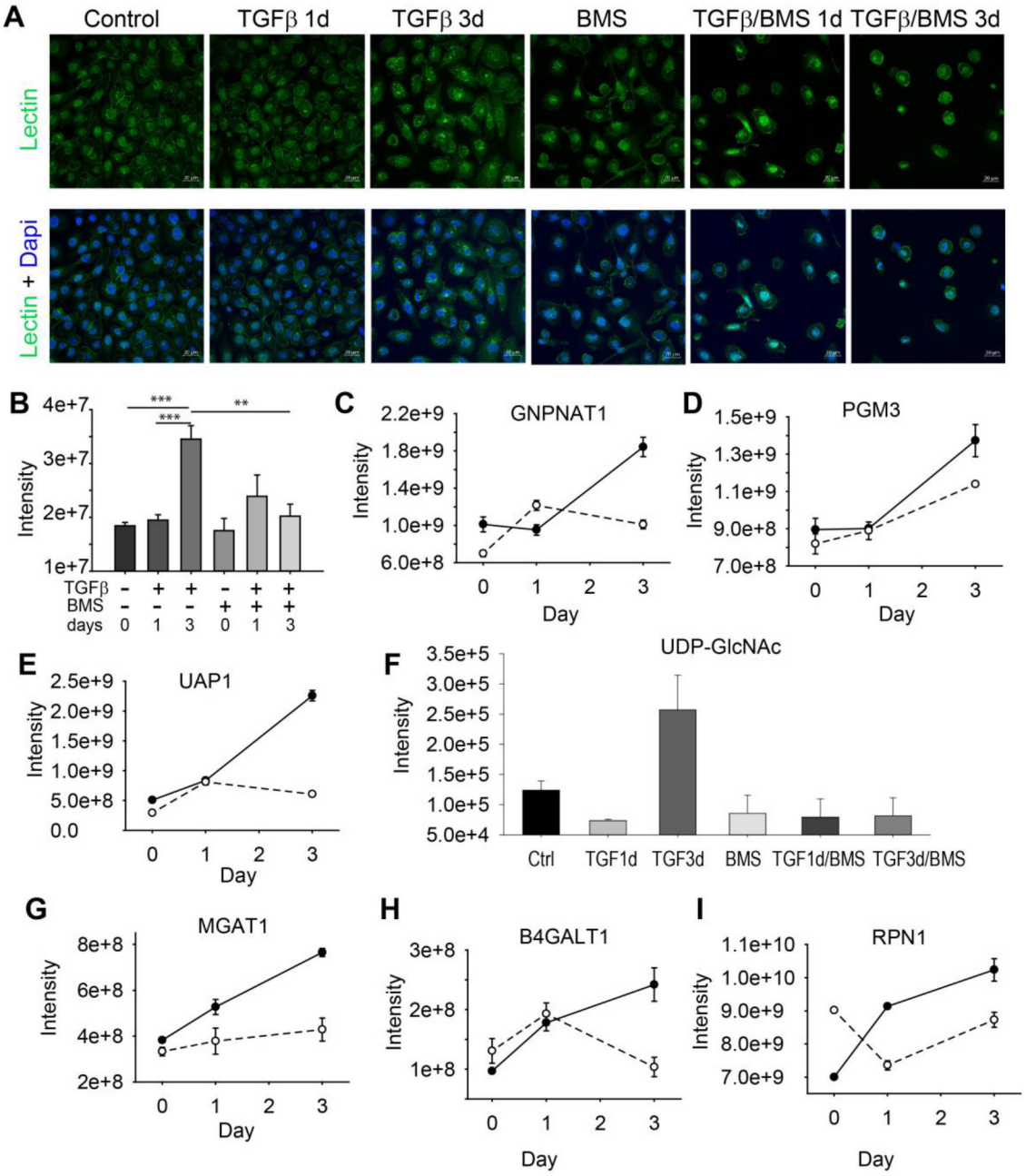

Figure 6. Activation of HBP pathway and protein N-glycosylation.

(A) Lectin staining of glycoproteins in hSAECs treated with TGFβ in the presence or absence of IKK inhibitor. The fixed cells were stained with DAPI for nuclei (blue) and lectin for glycoproteins (green) (magnified ×63). (B) Quantiification of lectin staining (n=6). (C)-(E) Time-series protein profiles of some HBP enzymes. The solid circle and line, the time-series profile of phosphopeptides in the absence of IKK inhibitor; the open circle and dot line, the time-series profile of phosphopeptides in the presence of IKK inhibitor; error bar, standard error. (F) Intracellular level of UDP-GlcNAc. t-test p-value: * $p<0.05$; **, $p<0.01$. (G)-(I) Time-series profiles of proteins regulating protein N-glycosylation.

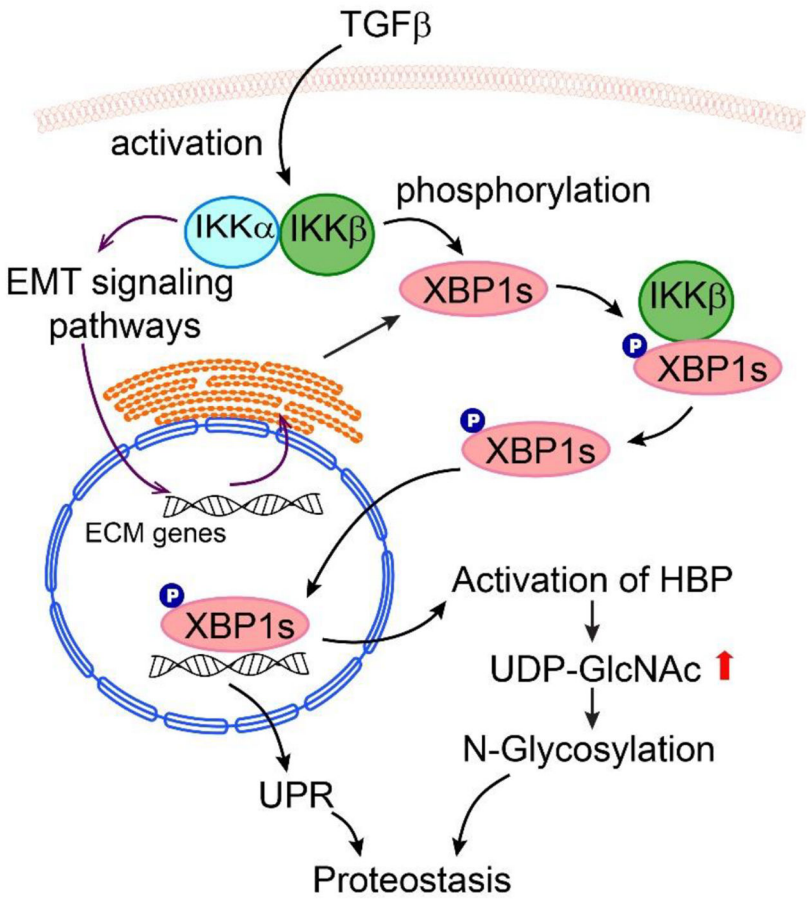

Figure 7.
IKK-XBP1-mediated glucose metabolism reprogramming regulates proteostasis and ECM production.